Thermochimica Acta 603 (2015) 69–78

Contents lists available at ScienceDirect

Thermochimica Acta

journal homepage: www.elsevier.com/locate/tca

Nanocalorimetry study of the evolution of melting characteristics of single layer silver alkanethiolate lamella: Fast heating/cooling and electrical annealing

Zichao Ye [a], Lito P. de la Rama [a,c], Liang Hu [a,d], Mikhail Y. Efremov [b], Leslie H. Allen [a,*]

[a] Department of Material Science and Engineering and Coordinated Science Laboratory, University of Illinios at Urbana-Champaign, Urbana, IL 61801, United States
[b] Department of Chemical and Biological Engineering, University of Wisconsin – Madison, Madison, WI 53706, United States
[c] SanDisk Corporation, Milpitas, CA 95035, United States
[d] Intel Corporation, Chandler, AZ 85226, United States

ARTICLE INFO

Article history:
Available online 4 September 2014

Keywords:
Nanocalorimetry
NanoDSC
Silver alkanethiolate
Single layer
Fast heating/cooling
Electrical annealing

ABSTRACT

Nanocalorimetry (NanoDSC) is applied to measure the melting characteristics of single layer silver pentadecanethiolate (AgSC15) crystals. Its attribute of high sensitivity enables the characterization of single layer species. The fast heating (~50,000 K/s) and cooling (~10^4 K/s) rates employed allow an *in situ* study of lamella layer evolution. By controlling the maximum temperature (T_{max}) achieved during heating/cooling cycles, the samples can be either melted or annealed. If T_{max} is larger than sample melting point (T_m), the first NanoDSC pulse shows the melting behavior of the as-synthesized crystal. The following rapid cooling (quenching) causes crystallinity loss. If T_{max} is smaller than T_m, electrical annealing takes place and partially recovers the quenched layered structure, but the melting enthalpy never reaches that of the first pulse.

1. Introduction

Nanocalorimetry (NanoDSC) [1–3] is a unique technique due to its ultra-fast heating rate (5000–200,000 K/s) and high sensitivity of specific heat (0.1 nJ/K) and enthalpy (1 nJ). This enables measurement of thermodynamic properties of very small amount (~50 ng)of materials, which is much less than the minimum mass (~mg) needed for conventional differential scanning calorimetry (DSC). The central part of NanoDSC is a chip-based calorimetry sensor (Fig.1a) fabricated on silicon wafer with a metal patterned silicon nitride membrane as the calorimetric cell. Nanocalorimetry was introduced in the 1990s and is now used worldwide [4–16]. Currently, NanoDSC has been applied to measure the thermodynamic properties of magic number metal clusters [17–21], glass transition (T_g) in polymer films [22], self-assembled monolayers (SAM) [23], metal silicides [24,25] and two-dimensional (2D) alkanethiolate layered crystals [26].

The rise of research in graphene [27] spawned the recent growing interest in other 2D layered materials with low aspect ratio [28,29]. These materials exhibit extraordinary size effect properties as the change of atomic/molecular layers. An interesting perspective of size effect phenomena in 2D layered systems lies in their melting behavior. Size-dependent melting finds its historical root in the 19th century with the pioneering theory of Gibbs–Thomson law [30]. This phenomenon has been observed in metal nanoparticles such as In [19,20], Sn [17] and Bi [21], as well as polymeric thin films [22]. Our recent work [26] on silver alkanethiolate (AgSCn, n = 7–18) lamellar crystals systematically extends this size effect melting to 2D layered systems, with single layer lamellae (~2–5 nm) as the thinnest species investigated. This is realized by the coupling of NanoDSC and a layer-control synthesis method [31,32].

AgSCn lamellar crystal was first synthesized by Dance et al. through a solution based chemical reaction [33]. Each single layer AgSCn has a bi-layer ribbon-like structure composed of a central plane of Ag-S network with alkanethiol chains extending on both sides [33–37]. Adjacent layers are bonded *via* van der Waals interaction, forming stacked AgSCn. The melting process of AgSCn involves an order-disorder phase transition due to the change of alkanethiol chain conformation from all-trans to partial gauche whereas the central plane structure is unaffected [26,38,39]. Currently, this organometallic lamellar crystal finds applications in the field of electronics [40], nanolithography [41] as well as biophysics [42].

* Corresponding author. Tel.: +1 217 356 3020; fax: +1 217 244 1631.
E-mail address: l-allen9@illinois.edu (L.H. Allen).

http://dx.doi.org/10.1016/j.tca.2014.09.001
0040-6031/

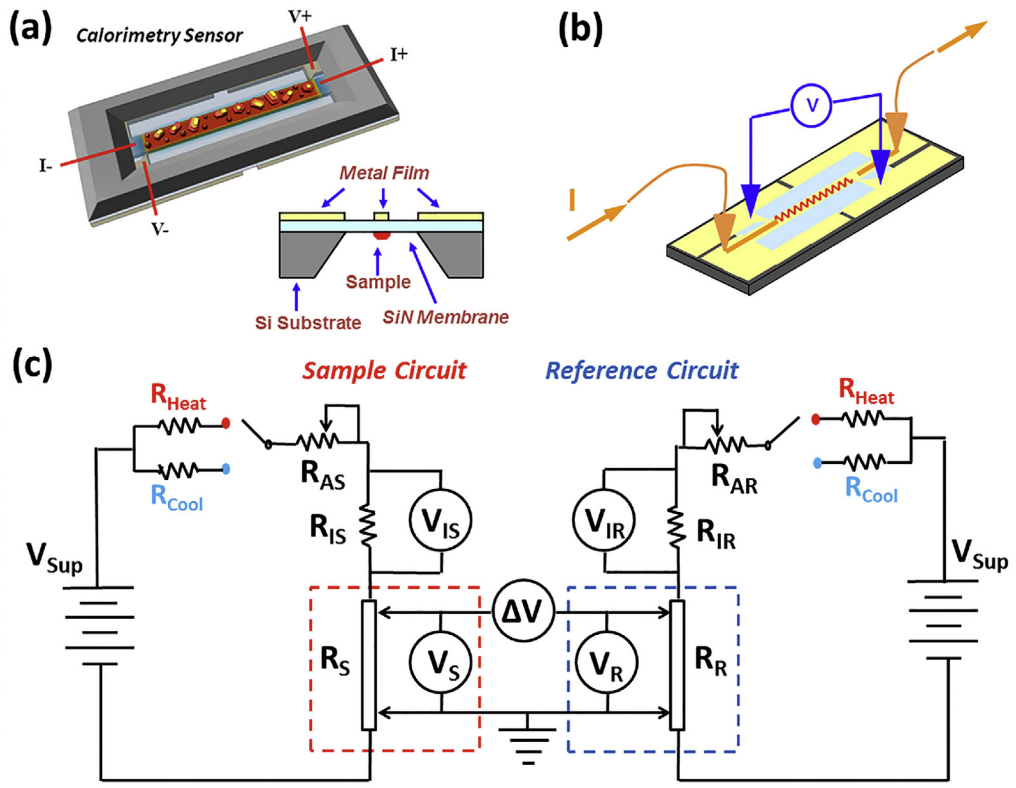

Fig. 1. (a) Bottom-view and cross-section schematic of the nanocalorimetry sensor. Si substrate: 500 μm thick; silicon nitride membrane: 100 nm thick; platinum metal film: 50 nm thick; platinum strip directly above sample: 0.5 mm wide [1]; (b) schematic of NanoDSC pulsing (front-side-view): C_p *vs.* T curve for every sensor is obtained *via* four-point probe measurement; (c) circuit diagram of differential mode NanoDSC. The region inside the red dashed box refers to Sample Sensor while the region inside the blue dashed box refers to Reference Sensor. R_{IS} and R_{IR} are the current determination resistance in the sample circuit and reference circuit, respectively. Heating rate is precisely controlled by adjusting R_{AS} and R_{AR} values. The switches shown can be changed between regular pulsing mode and cooling mode. (For interpretation of the references to color in this figure legend and text, the reader is referred to the web version of this article.)

In our prior work [26], size effect melting of AgSCn layered crystals is observed from two degrees of freedom. Single layer AgSCn shows a discrete increase of melting point T_m (total $\Delta T \approx 20\,^{\circ}C$) as the integer increments of alkanethiol chain length ($n = 7$–18). Stacked AgSCn layers exhibit an odd/even melting effect as well as a layer-number-dependent collective melting in which crystals with larger number of layers melt at higher T_m. This is the first time that chip-based calorimetry is employed to investigate 2D layered materials. The successful measurement of single layer melting highlights the possibility of studying extremely thin materials *via* NanoDSC, which is unique in that conventional DSC is only designed for bulk materials where size effect is negligible.

In this paper, *in situ* multiple NanoDSC pulses are carried out on single layer silver pentadecanethiolate (AgSC15) crystals. The first pulse represents the melting behavior of the original crystals. The second and subsequent multiple pulses show irreversible loss of crystallinity under such fast heating (~50,000 K/s) and cooling (~10^4 K/s [25]) rates. Electrical annealing technique is introduced and is able to recover the value of T_m but the heat of fusion (H_m) of quenched samples never reaches that of the first pulse. As a comparison, conventional DSC is employed to analyze bulk multilayer AgSC15 samples. Unlike NanoDSC, reversible melting of bulk AgSC15 is revealed because of the relatively low heating/cooling rate (~10 K/min) used. As a consequence, NanoDSC proves itself to be a unique technique in the thermodynamic analysis of 2D layered materials in terms of three aspects: (1) melting characteristics of single layer species can be easily resolved; (2) its ultra-fast nature enables *in situ* investigations of layer evolution during heating/cooling cycles; (3) electrical annealing is a potential tool for crystallinity recovery.

2. Experimental

2.1. Synthesis

2.1.1. Materials

Silver pellets (99.99%) obtained from Kurt J. Lesker Co., are used as silver source for physical vapor deposition. Silver nitrite powder ($AgNO_3$, ≥99.0%), acetonitrile (99.8%), triethylamine (≥99.0%), 1-pentadecanethiol (1-$C_{15}H_{31}SH$, ≥98%) and 1-hexadecanethiol (1-$C_{16}H_{33}SH$, ≥99%) used in this study are purchased from Sigma–Aldrich Co., and used without further purification. Toluene (≥99.5%) is used as received from Macron Fine Chemicals Co.

2.1.2. Synthesis of single layer AgSC15

Single layer AgSC15 crystals are prepared from a layer-control synthesis method on NanoDSC sensors (SiN_x surface). The detailed procedures are described in our previous publications for both single-layer [32] and stacked-layer samples [31]. Fig. 2 briefly illustrates the synthesis procedure of single layer AgSCn. The final product is precisely determined by the amount of silver deposited at the first synthesis stage and the furnace annealing temperature in the last step.

The deposition of silver (step 1 in Fig. 2) is carried out in a thermal evaporator at a base pressure of 5×10^{-8} Torr. The exact amount of silver deposited is estimated by a quartz crystal

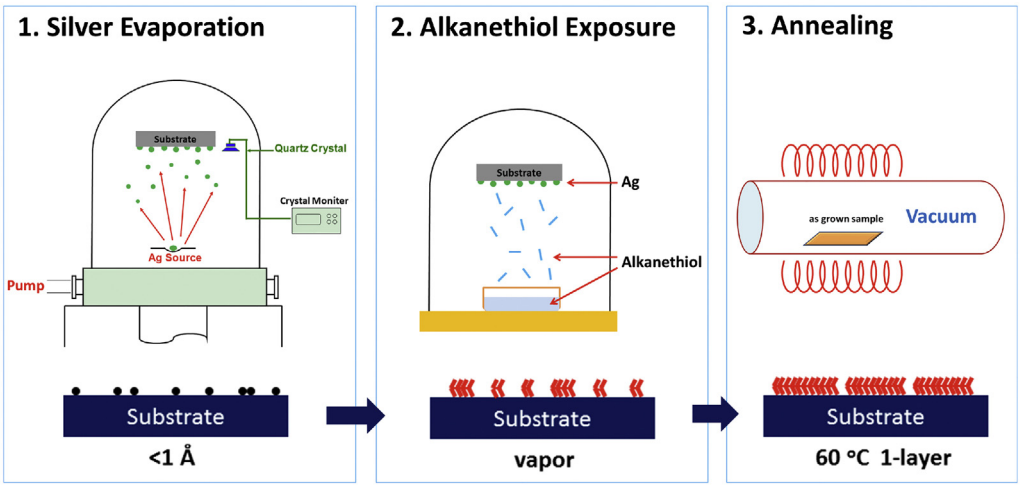

Fig. 2. Schematic of synthesis procedures for single layer AgSCn: (1) thermal evaporation of silver clusters with certain equivalent thicknesses; (2) reaction between as-deposited silver and alkanethiol vapors to form as-grown AgSCn; (3) annealing to form final large 1-layer AgSCn crystals with low aspect ratio.

monitor (QCM) measuring rate and a photodetector coupled shutter that accurately determines deposition time. In this study, the as-deposited silver is exposed under 1-pentadecanethiol vapor for 3 days (step 2 in Fig. 2). This vapor method is efficient for the synthesis of AgSCn with single or several layers. The as-grown AgSC15 samples are annealed in a vacuum furnace at a base pressure of 1×10^{-7} Torr (step 3 in Fig. 2). The growth of single layer AgSC15 requires a strict synthesis condition of silver amount (equivalent thickness) less than 1 Å and annealing temperature at about 60 °C.

2.1.3. Synthesis of as-grown AgSC16

Based on the synthesis of single layer AgSCn, gradual increase of deposited silver thickness and annealing temperature result in the pile up of 1-layer species, forming stacked or multilayer AgSCn [32]. The as-grown AgSC16 lamellae described as a preliminary example for electrical annealing technique (Section 3.3) is synthesized using a silver amount of ~5 Å. Details are described in our previous work [31]. For comparison, the as-grown sample is then furnace annealed to 90 °C in a vacuum tube as shown in Fig. 2 (step 3) or electrical-annealed to 124 °C *via* NanoDSC pulses.

2.1.4. Synthesis of bulk AgSC15 sample

Bulk multilayer AgSC15 sample is synthesized from a solution based chemical reaction method, mainly following the contributions of Levchenko et al. on synthesis and recrystallization [39]. Briefly, $AgNO_3$ in acetonitrile (125 mM) is gradually added (1 mL/min) to an acetonitrile solution of equimolar 1-pentadecanethiol (250 mM) and triethylamine (250 mM). The mixture is stirred overnight without light exposure. The precipitate (bulk AgSC15) is collected after suction filtration and washed with acetonitrile (3 times). Large grain sizes and aggregations are observed in the powder with a color of yellowish white. To improve the crystallinity of the product, a recrystallization process is applied. AgSC15 powder is first dissolved in hot toluene at a temperature of 90–100 °C. The hot solution (transparent, yellow) is then naturally cooled down to room temperature with AgSC15 gradually separates out from toluene. The followed cooling in ice water guarantees a complete precipitation of AgSC15. After suction filtration and sample washing, the final product is dried overnight for characterization. The final AgSC15 powder is mainly pinkish brown. X-ray diffraction results indicate the crystallinity of bulk AgSC15 is dramatically improved after recrystallization (data not shown).

2.2. Sample Characterization

2.2.1. NanoDSC measurement of single layer AgSC15

Details of NanoDSC technique are published in our previous work [1–3]. NanoDSC sensor shown in Fig. 1a is a chip-based device fabricated on a silicon wafer (500 μm). A low stress silicon nitride membrane (100 nm) patterned with platinum thin film (50 nm) on one side constitutes the low thermal mass calorimetric cell. In this study, each blank sensor is annealed to 450 °C to stabilize before use. AgSCn samples are deposited on the opposite side of metal film. A self-aligned shadow mask is applied to confine the deposition of samples to the certain region directly beneath metal strip to reduce the error caused by the loss of materials [43]. The metal strip performs as both a heater for joule heating when current pulses are applied and a thermometer whose temperature coefficient of resistance (TCR) is calibrated before any experiment. Fig. 1b shows a typical schematic of NanoDSC set-up with a real time four-point probe measurement. Fig. 1c illustrates the circuit diagram of NanoDSC. NanoDSC measurements are carried out in a differential mode under a vacuum of 5×10^{-8} Torr. During scans, synchronized current pulses are generated separately from the two power supplies in the sample circuit and the reference circuit. Typical sensor resistances are 50–100 Ω and the circuit current ranges from 10 to 50 mA [3]. Heating rate is precisely controlled by tuning R_{AS} and R_{AR}. The measured sample heat capacity is roughly proportional to the derivative of ΔV over time [3]. The final calorimetric curve (sample heat capacity C_p *vs.* T) is obtained after 1st, 2nd and 3rd baseline subtraction of addenda correction, blank cell correction and heat loss correction, respectively [2]. A switch is used to change the circuit between regular pulsing mode and cooling mode, which measures the temperature drop as a function of time during cooling by applying a small current (1–5 mA) through NanoDSC sensor. Only the pulsing mode is used in this study and the cooling mode will be discussed in future publications.

In this research, each current pulse applied for sample calorimetric measurement last 3.7 ms, during which the temperature of 1-layer AgSC15 increases from room temperature to about

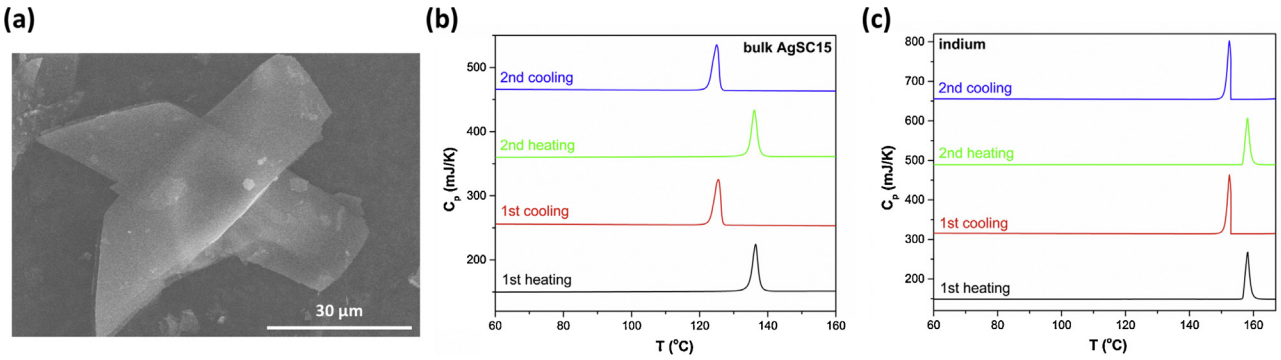

Fig. 3. (a) SEM image of bulk AgSC15 multilayer crystals; (b) DSC results of bulk AgSC15 (1.4 mg) for two heating/cooling traces; (c) DSC results of indium sample (6.8 mg) for two heating/cooling cycles during DSC calibration. For both (b) and (c), only the black curves are not vertically shifted. The sample-to-sample variation of C_p is about ±75 mJ/K. Although such a huge error does not affect the measured T_m and H_m, DSC 4000 is not a perfect calorimetry for specific heat measurement. The variation of reproducibility for a specific sample is less than 0.05 mJ/K.

200 °C (~50,000 K/s). Typical material amount calculated is less than 50 pmol or 20 ng. Specifically, NanoDSC measurements on AgSC15 samples are conducted in the following steps using the set-up shown in Fig. 1b and c: (a) 1st single calorimetric pulse to 200 °C, (b) 2nd single calorimetric pulse to 200 °C, (c) subsequent 50 pulses to 200 °C, (d) electrical annealing to 100 °C for 50 pulses (1.6 ms/pulse), (e) 1 calorimetric pulse to 200 °C after electrical annealing, (f) electrical annealing to 110 °C for 50 pulses (1.8 ms/pulse), and (g) 1 calorimetric pulse to 200 °C after electrical annealing. For steps (c), (d) and (f), the whole heating/cooling cycle time for each pulse is set to be 1 s (the interval between the occurrence of two adjacent pulses is 1 s). Following thermodynamic information can be extracted from the obtained C_p *vs.* T curves during each pulse: T_m (peak position), H_m (peak area), full-width-half-maximum (FWHM) of the peak and amount of sample (divided the shift in C_p baseline at the temperature region higher than T_m by sample specific heat). The amount of AgSCn is also estimated by measuring silver amount using QCM and RBS by assuming that the stoichiometric ratio of Ag and AgSCn presented is 1:1. In addition, material amount can also be estimated by measuring the volume of AgSCn using AFM histogram, as is shown in our previous work [32].

2.2.2. Conventional DSC measurement

Conventional DSC measurements on bulk AgSC15 multilayer samples are conducted using Perkin-Elmer Standard Single-Furnace DSC-4000 with aluminum sample pans. It works under differential mode with a temperature resolution of ±0.1 °C and a calorimetric error of ±2%. Typical sample mass used is 3–5 mg and the heating/cooling rate is set to be 10 K/min. Temperature and sensitivity calibrations are done by indium and zinc before experiments. In this study, bulk AgSC15 samples are scanned from room temperature to 170 °C for two thermal cycles.

2.2.3. Scanning Electron Microscope (SEM)

The morphology of bulk AgSC15 is studied using a Hitachi S4700 SEM with an accelerating voltage of 20 kV. Since the organic portions of AgSCn layers are very sensitive to the long-time exposure of electron beam radiation, SEM graphs are always taken immediately after moving the microscope to certain target areas [31].

3. Results and discussion

3.1. Characterization of bulk AgSC15 crystals

Fig. 3a shows the SEM image of bulk AgSC15 crystals. Each lamellae platelet has an areal dimension of about 1000 μm^2. The total thickness of the multilayer structure revealed by the Scherrer analysis of X-ray diffraction data is less than 400 nm with an individual lamella thickness of 41.71 ± 0.05 Å, which is consistent with our previous work on surface grown crystals [26]. Such crystal morphology and structure of low aspect ratio in AgSC15 is similar to other bulk AgSCn samples with even alkanethiol chain length reported in literature [36,38,39].

DSC data of two thermal cycles are illustrated in Fig. 3b. This is the first reported DSC results of bulk AgSCn with odd alkanethiol chain length. Thermodynamic parameters of the four DSC traces are tabulated in Table 1.

The error bars are obtained from the variation between different bulk AgSC15 samples. The 20% error obtained for molar enthalpy is much larger than the one measured in standard indium under the same condition and the reason is not determined at this time. The melting point revealed from heating traces is consistent with that of multilayer samples grown on substrates (136.5 °C) [26]. Upon cooling, a decrease of T_{peak} (ΔT~11 °C) is observed as compared with that of heating trace (Table 1). Such shift of T_{peak} (ΔT~4 °C) is also found for standard In sample during DSC calibration (Fig. 3c). Since thermal lag effect only depends on scanning rate (10 K/min), sample property, thermal contact and instrument conditions [44], the heating and cooling traces for a particular sample should show same degree of thermal lag, which is estimated to be less than 1 °C from In temperature calibration. Moreover, little thermal lag is observed in the melting of AgSC15 crystals. Thus the huge shifts of T_{peak} ($\Delta T >> 1$ °C) between heating and cooling traces shown in Fig. 3b and c are mainly attributed to the super-cooling effect of materials. The super-cooling of In is about 4 °C, which is consistent with the one reported in literature [45], whereas the super-cooling of AgSC15 is measured to be about 11 °C. The molar enthalpy calculated from either endothermic heating or exothermic cooling has similar values and is independent of thermal cycles. This indicates the reversibility in the phase transition of bulk AgSC15 at around 136 °C. The low heating/cooling rate (10 K/min) of DSC cycles allows a complete recrystallization of melted crystals during cooling process. Such reversible thermodynamic character was also previously observed

Table 1
DSC on bulk AgSC15 (10 K/min).

Thermal cycle	T_{peak} (°C)	H_m (kJ/mol)	FWHM (°C)
1st heating	136.6 ± 0.2	52.4 ± 10.2	2.3 ± 0.5
1st cooling	125.3 ± 0.3	52.4 ± 10.4	2.3 ± 0.1
2nd heating	136.4 ± 0.3	52.2 ± 10.5	2.3 ± 0.4
2nd cooling	125.0 ± 0.1	51.8 ± 10.8	2.4 ± 0.3

in bulk AgSC8, C10, C12, C16 and C18 samples [38,39]. The molar enthalpy value of bulk AgSC15 is consistent with the one extrapolated from those for AgSC12 and AgSC16 [38,39]. This further confirms the inference that transition enthalpy scales with the alkanethiol chain length [39]. The FWHM of the transition peak is probably due to the limitation of the instrument since DSC measurement on standard indium samples also shows a FWHM of 1.5 °C for heating/cooling rates of 10 K/min.

3.2. The effect of fast heating and cooling on the melting and solidification of lamella

In contrast to conventional DSC, NanoDSC is capable of resolving the thermodynamic characteristics of single layer AgSCn crystals (~15 ng). The lamella nature of single layer AgSC15 grown on NanoDSC sensor has been verified by our group through AFM, XRR and XRD [32]. Melting behaviors of single layer AgSC15 reported in our prior publication [26] is extracted from the first NanoDSC pulse, which best represents the phase transition (T_m = 119.2 °C) of as-synthesized samples with uniform crystallinity and in-plane ordering.

The effect of fast cooling of NanoDSC highlights its significance when multiple melting/cooling cycles are investigated. The molten crystal after the first pulse quenches to room temperature from about 200 °C at a fast cooling rate (~10^4 K/s). Results of the real time evolution of heating curves (C_p *vs.* T) as a function of pulse number for 1-layer AgSC15 are shown in Fig. 4a. It includes the 1st pulse, 2nd pulse and subsequent 50 pulses. Values of T_m, H_m and FWHM for each curve are summarized in Fig. 4b,c and d, respectively. T_m value dramatically shifts to a lower temperature (ΔT~3 °C) at the second pulse and remains almost unchanged during the subsequent multiple thermal cycles as compared with the first pulse. The error bars in Fig. 4b refer to the instrumentation statistical variations arising from sample-to-sample errors (±1.5 °C) [26]. There is in total about 50% reduction of H_m from the as-synthesized crystals to the subsequent quenched crystals (Fig. 4c).

Unlike the fast cooling, fast heating rate has little effect on the melting characteristics of layered crystals, as is evidenced in our prior work [26] that shows same values for T_m and H for both DSC (10 K/min) and the first pulse of NanoDSC (50,000 K/s). However, since crystal solidification strongly depends on the cooling rates, it

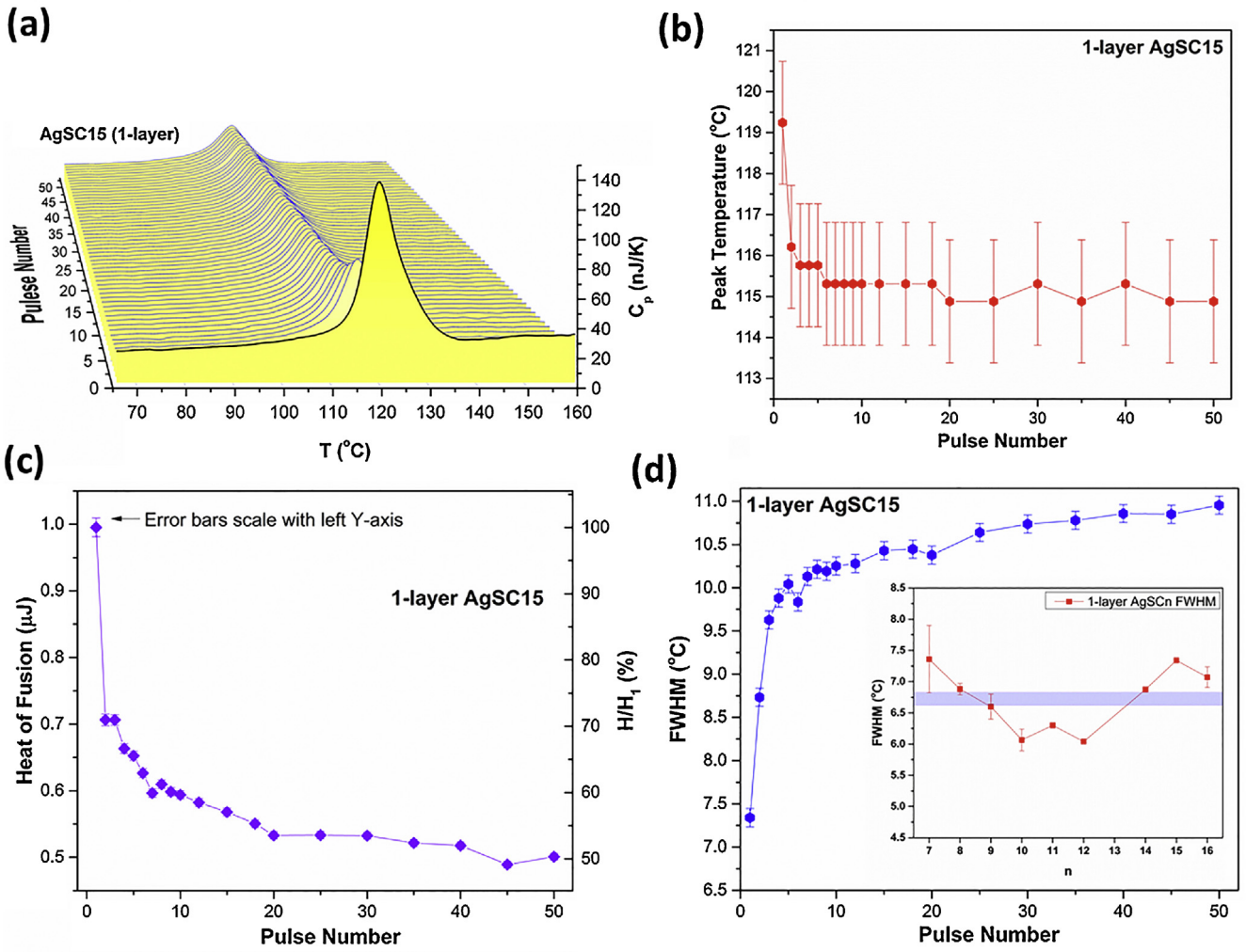

Fig. 4. (a) Plot show the real time evolution of C_p *vs.* T curves during multiple NanoDSC pulses for single layer AgSC15. (b)–(d) Plots show the peak temperature (T_m), heat of fusion H_m, and peak FWHM as a function of pulse number during multiple NanoDSC pulses in (a) for single layer AgSC15. The inset of (d) shows the FWHM values of the first pulses for monodisperse as-synthesized 1-layer AgSCn crystals (n = 7–16, synthesized using the procedure shown in Fig. 2) as a function of alkanethiol chain length n. The blue strip with a value of 6.7 ± 0.1 °C represents the average of all the red data points. (For interpretation of the references to color in this figure legend and text, the reader is referred to the web version of this article.)

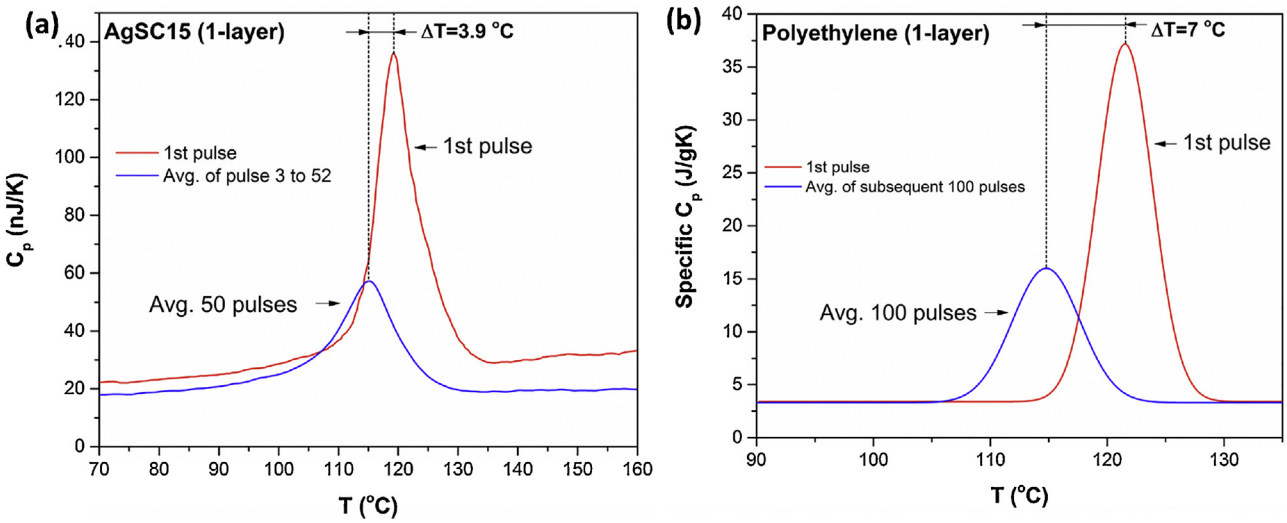

Fig. 5. (a) NanoDSC calorimetric curves for 1-layer AgSC15: 1st pulse (red) and the average curve of the 3rd pulse to the 52nd pulse (blue); (b) NanoDSC calorimetric curves for 1-layer polyethylene crystals: 1st pulse (red) and the average curve of the subsequent 100 pulses (blue). Data for this plot are extracted based on Fig. 3a in our prior publication [46]. (For interpretation of the references to color in this figure legend and text, the reader is referred to the web version of this article.)

is the solidification during quenching right after the first pulse that alters the originally well-defined single layer AgSC15. The quenching cools the crystal from molten state to a solid state within 100 ms, causing crystallinity loss. As a consequence, the lamella that is heated during subsequent pulses has no longer the crystallinity as the one before the first pulse.

It is important to note that during multiple melting/cooling cycles, there is a systematic increase of melting peak FWHM (Fig. 4d) for single layer AgSC15. The value for the first pulse is 7.3 °C, which is close to the typical FWHM values for all 1-layer AgSCn (n = 7–16) shown in Fig. 4d inset [26]. All these values range from 6 to 7.5 °C and the blue strip estimates their average of 6.7 ± 0.1 °C. This indicates that multiple thermal cycles significantly broaden the melting peak. Instrumentation broadening (due to sensor temperature gradient, resolution limitation, etc.) is only about 3 °C, as is verified by NanoDSC measurement on standard indium samples [3,20]. Kinetic issues of fast heating rate is not considered as the reason for peak broadening as the FWHM of indium melting peak from NanoDSC (~3 °C) and DSC (~1.5 °C) are within experimental error. Most of the peak broadening in this study is attributed to the variation in lamella thickness/size coupled with size-dependent melting of AgSCn crystals [26]. This indicates that crystallinity loss during multiple melting/quenching cycles significantly changes the size uniformity of 1-layer AgSC15 crystals.

Fig. 5a shows the melting peaks of 1-layer AgSC15 in this study (red: 1st pulse; blue: average of the 3rd pulse to the 52nd pulse). The plot agrees with the results shown in Fig. 4. The shift of C_p between the red curve and the blue curve after melting is possibly caused by the degasing of sensor as there may be desorption of alkanethiol molecules. Based on our prior NanoDSC research [46], the crystallinity loss of layered materials is also observed in single layer polyethylene crystals. Fig. 5b illustrates the calorimetric curves for the first pulse and the average of subsequent 100 pulses on single layer polyethylene *via* NanoDSC. Comparable to 1-layer AgSC15, multiple melting/quenching cycles after the first pulse on polyethylene lamella also lead to a 50% reduction of H_m, ~7 °C of T_m shift and ~1.5 °C of FWHM broadening. The crystallinity loss of the single layer polyethylene is confirmed by our previous transmission electron microscopy results as a well-defined diffraction pattern is observed before the first pulse, whereas no diffraction pattern is observed after NanoDSC cycles [46]. Similar phenomenon is also reported by Grubb et al. [47] *via* real time small-angle X-ray diffraction on polyethylene. They noticed that quenching from high temperatures causes rapid recrystallization and changes of lamella thickness.

3.3. Electrical annealing technique

Electrical annealing is achieved by joule heating using the same hardware as is used for the NanoDSC fast scanning (Fig. 1). Electrical annealing by joule heating is controlled by a series of current pulses applied to the metal film on NanoDSC sensors. Consequently, the metal film heats the sample *via* conduction through SiN_x membrane. Its maximum temperature is lower than sample T_m. The annealing temperature is controlled by the magnitude of current and the duration of pulsing time, and the heating rate is extremely fast (>5 k K/s). In contrast, the other method of annealing employed in this work is “furnace annealing”

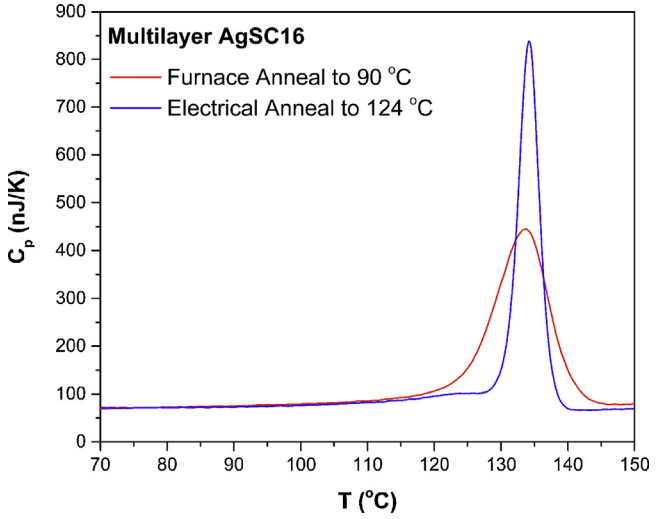

Fig. 6. NanoDSC calorimetric results for multilayer AgSC16 samples after furnace anneal to 90 °C (red curve) and after electrical anneal to 124 °C (blue curve). (For interpretation of the references to color in this figure legend and text, the reader is referred to the web version of this article.)

Table 2
Comparison between the effects of furnace annealing and electrical annealing on as-grown AgSC16.

Curves in Fig. 6	T_m (°C)	H_m (μJ)	FWHM (°C)
Furnace anneal to 90 °C	133.8	3.59	9.0
Electrical anneal to 124 °C	134.1	3.59	3.6

(step 3 of Fig. 2), in which the NanoDSC sensors (with samples) are transferred into a vacuum furnace oven where sample heating occurs with extremely slow heating rates of less than 1 K/min. Heat transfer to the sample occurs by infrared radiation. Electrical annealing is unique due to its fast heating/cooling rates (anneal samples within milliseconds), *in situ* characteristics (no sample transfer between annealing and NanoDSC measurement) and more precisely controlled temperature programs (no overshooting of temperature). The broad range of heating rates of the electrical annealing technique allows a wide range of annealing schedules. This enables us to deconvolute multiple intrinsic thermal processes present in materials (*e.g.*, nucleation *vs.* growth).

As an example, preliminary results shown in Fig. 6 illustrate the comparison between the first calorimetric pulses after electrical annealing (124 °C) and furnace annealing (90 °C) on as-grown AgSC16 lamellae (T_m = 129.8 °C [31]). Both annealing temperatures are lower than sample T_m so that only layer crystallization and growth occur during annealing and no material melts. The calorimetric parameters for the C_p *vs.* T curves are tabulated in Table 2.

Based on the size-effect melting, the increase of T_m after annealing infers the pile up of as-grown AgSC16 lamellae, forming multilayer crystals [26]. The similarity of T_m and H_m between furnace annealed and electrical-annealed samples indicates their equivalence, though their annealing temperatures are different. Electrical annealing significantly narrows the melting peak width to 3.6 °C, which is among the smallest FWHM values we can obtain from NanoDSC. This value (3.6 °C) approaches the limit of instrumentation broadening [3,20] and may be a result of a small dispersion of lamellae thickness. In contrast, furnace annealed crystals have various thicknesses (relatively large dispersion) as the limited annealing temperature range available for layer-control in multilayer samples [26]. Therefore, electrical annealing is potentially more accurate in layer-control and is a possible alternative to furnace annealing in the use of material growth.

Electrical annealing (100 °C and 110 °C) is performed on quenched single layer AgSC15 samples for the purpose of recrystallization and crystallinity recovery. Fig. 7a illustrates the temperature profile for one heating/cooling cycle of NanoDSC scan that measures sample melting properties. The maximum temperature achieved is 197 °C, higher than sample T_m. Multiple NanoDSC melting/cooling cycles shown in Fig. 4 is achieved by repeating this NanoDSC scan multiple times. Each pulse re-melts the sample that is recrystallized from the cooling of the last cycle and thus the effect of recrystallization does not accumulate. In contrast, Fig. 7b illustrates the temperature profile for 50 identical cycles of scans for annealing with a maximum temperature of 110 °C, lower than sample T_m. This allows an accumulation of the effect of recrystallization that occurs during each cooling process. The effect of recrystallization can be studied by introducing a NanoDSC pulse to 197 °C after electrical annealing (Fig. 7b). Assuming that recrystallization is considered to be significant only when the sample temperature is larger than 50 °C during cooling, the total recrystallizing time for electrical annealing to 110 °C with 50 cycles is added up to be 1.1 s. This is much longer than the one for NanoDSC scans to 197 °C, where valid recrystallization only lasts 37 ms during the cooling of an individual cycle. It is the difference in the maximum temperature ($<T_m$ *vs.* $>T_m$) of these two NanoDSC processes that results in the different effects on sample evolution (recrystallization *vs.* melting/recrystallization/re-melting). Even though sample crystallinity is damaged during multiple melting/cooling cycles (Fig. 4), multiple electrical annealing pulses afterwards are potentially useful for crystallinity recovery.

Fig. 8a shows the C_p *vs.* T curves for the first pulse after 100 °C (orange) and 110 °C (green) electrical annealing. Comparing with the average melting curve for multiple (3rd–52nd pulse) calorimetric pulses (blue), we notice that, as a result of electrical annealing, T_m gradually reverts back to that of as-synthesized crystals and peak FWHM significantly reduces to a value even narrower than that of initial first pulse. However, H_m never recovers as it remains almost the same as that of quenched crystals.

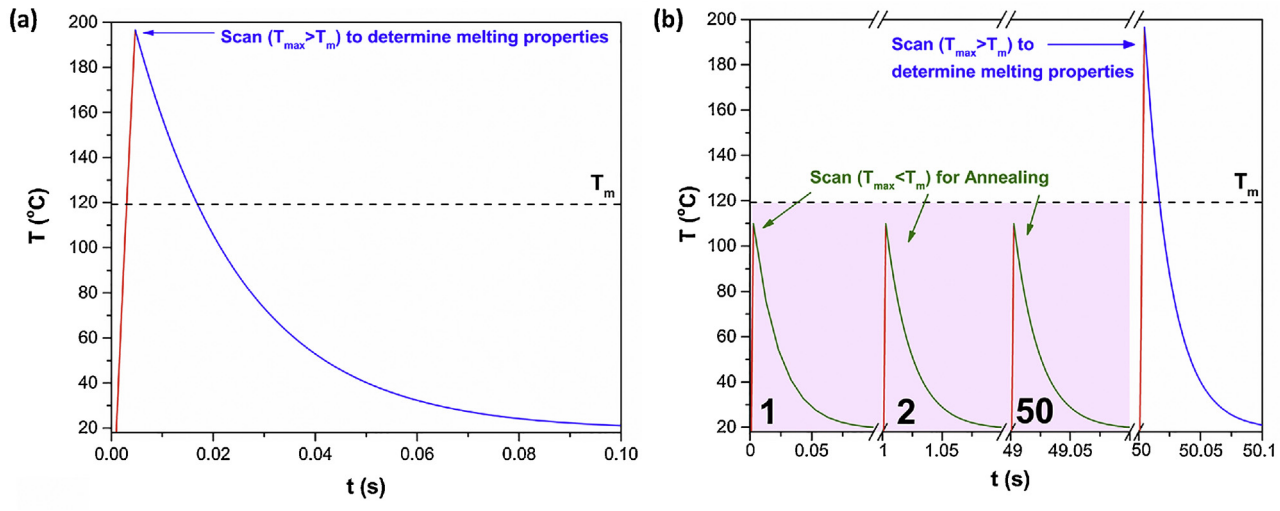

Fig. 7. (a) The T *vs.* t profile (heating: red curve; cooling: blue curve) for a NanoDSC scan (T_{max} = 197 °C > T_m) to measure the melting properties of 1-layer AgSC15 crystals; (b) 50 identical NanoDSC scans (T_{max} = 110 °C < T_m) for annealing (electrical annealing), as is shown in the pink box (heating: red curve; cooling: green curve). A NanoDSC scan to T_{max} = 197 °C after electrical annealing is employed to determine the melting properties on electrical-annealed samples. The black dashed line represents the T_m of the sample (119.24 °C). The heating profile for both processes are measured using the same heating rate of 50,000 K/s. Passive cooling profiles are estimated from Newton's Law of cooling [48] using an initial cooling rate of 10^4 K/s [25]. (For interpretation of the references to color in this figure legend and text, the reader is referred to the web version of this article.)

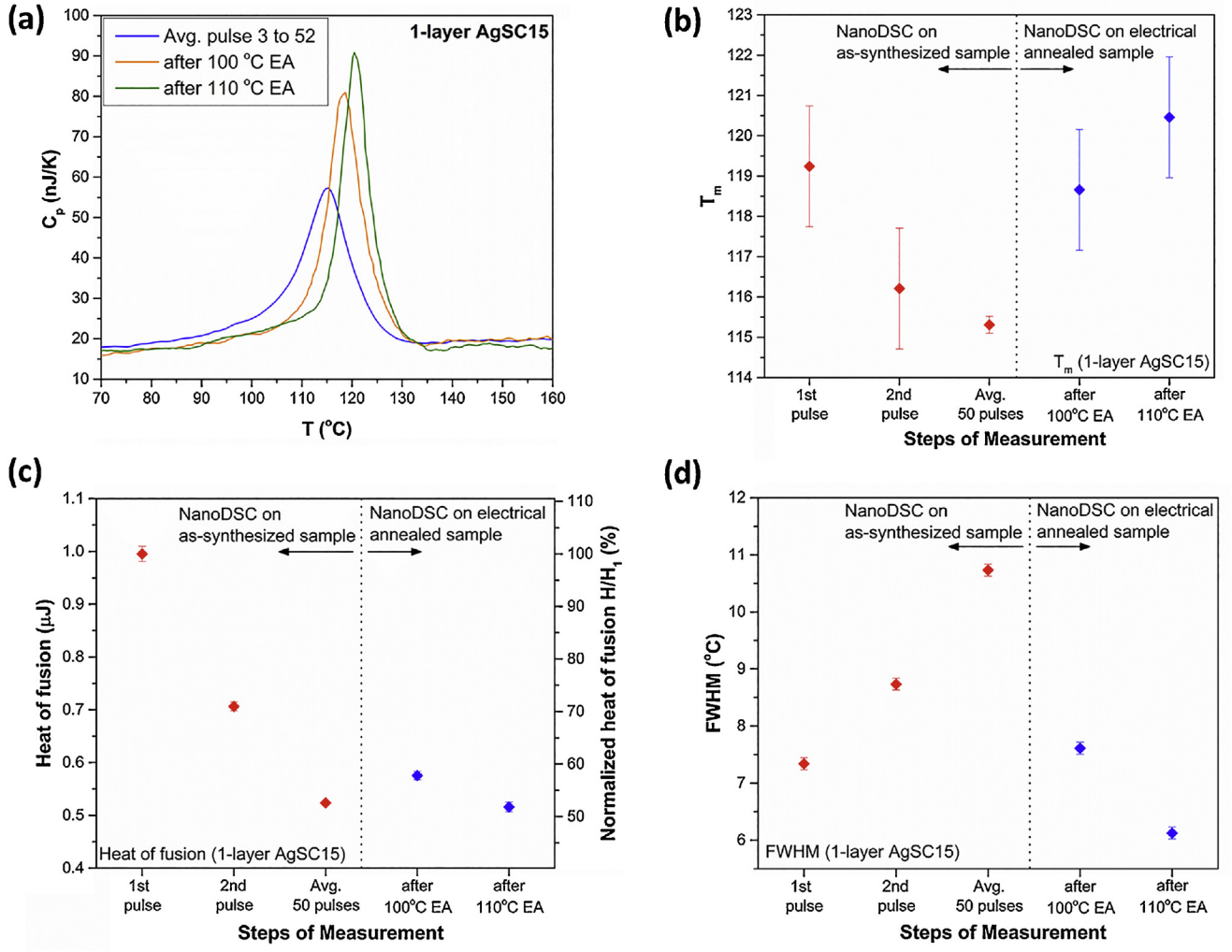

Fig. 8. "EA" is short for "Electrical Annealing". (a) NanoDSC results for 1-layer AgSC15: the average curve of the 3rd pulse to the 52nd pulse (blue, same as the blue curve in Fig. 5a), first pulse after 100 °C electrical annealing, first pulse after 110 °C electrical annealing. (b), (c) and (d) show the evolution of T_m,H_m and endothermic peak FWHM, respectively, during the sequential steps of NanoDSC measurement in this study. The X-axis of the five data points represents the 1st calorimetric pulse to 200 °C, 2nd calorimetric pulse to 200 °C, average of subsequent 50 calorimetric pulses to 200 °C, 1 calorimetric pulse to 200 °C after 100 °C electrical annealing, and 1 calorimetric pulse to 200 °C after 110 °C electrical annealing, respectively. (For interpretation of the references to color in this figure legend and text, the reader is referred to the web version of this article.)

The overall evolutions of T_m, H_m, and FWHM during the whole sequential steps of NanoDSC measurement are summarized in Fig. 8b–d respectively. The first 3 data points of each plot show the results of multiple-calorimetric pulses (52 pulses) to about 200 °C on as-synthesized single layer AgSC15, whereas the 4th and 5th data points represent the ones for single-calorimetric pulses to about 200 °C on 100 °C and 110 °C electrical-annealed samples, respectively. A higher annealing temperature yields crystals with a higher T_m and a narrower peak width. As expected, the annealed samples degrade back to the typical quenched state after any pulse. Similar results are also observed in the electrical annealing on quenched single layer polyethylene [46]. In this case, a controlled temperature ramp rate is obtained by incrementally applying discrete, low-current pulses. No multiple thermal cycles are used. NanoDSC measurements also show a recovery of T_m but the H_m is still low.

3.4. Possible suggestions for lamella evolution

For the explanation of the above *in situ* NanoDSC results, possible explanations for layer evolution are suggested.

Upon the melting of single layer AgSC15 crystals during the first pulse, gauche defects are introduced into the originally all-trans alkanethiol chains [38,39]. Only part of the crystallinity reverts back during the following quenching due to the kinetic attributes of fast cooling: some gauche conformers do not have enough time to relax back to the stable well-defined all-trans conformers. As a consequence, only the segment of alkanethiol chain (effective chain length) that has all-trans conformation is involved in the melting during the next pulse. According to our prior results that the T_m of single layer AgSCn decreases as the reduction of alkanethiol chain length (n) [26], lamella with a shorter effective chain length after quenching should melt at a lower temperature as compared with the as-synthesized AgSC15 crystals with 15 all-trans methylene/methyl groups in each chain. This is well consistent with the observation shown in Fig. 4b. During the subsequent calorimetric melting/cooling cycles (2nd–52nd), lamella structure evolves in a repeated sequence of partial recrystallization, melting and partial recrystallization. Thus the effective chain lengths at the end of any melting/cooling cycles are almost the same. This explains why there is not a huge variation in T_m values from the 2nd pulse to the 52nd pulse (Fig. 4b). Periodic

electrical annealing to a temperature lower than T_m gains enough time for the recrystallization of all the gauche conformers back to all-trans conformers so that annealed samples can have almost the same T_m as as-synthesized crystals (Fig. 8b). We infer that upon quenching, different alkanethiol chains in lamella may be recrystallized at different rates. This leads to a dispersion of effective chain lengths and they will melt at slightly different temperatures. This explains the broadening of melting peak FWHM during multiple calorimetric measurements (Fig. 4d). The reduction of lamella thickness dispersion *via* electrical annealing expectedly narrows the FWHM (Fig. 8d).

The evolution of H_m (Fig. 8c) in this study may be explained by alkanethiol desorption or decomposition of single layer AgSC15. The ~40% change of C_p between the red curve and the blue curve in Fig. 5a is a possible indication of this effect. From Fig. 4c, we suggest that desorption occurs during all the NanoDSC scans after the first pulse but to a less degree as thermal cycles proceed. Such desorption during NanoDSC pulses has been observed in SAM on Au [23], which is also a monolayer species. Electrical annealing never recovers H_m (Fig. 8c) since the loss of materials *via* desorption or decomposition is irreversible.

Other suggestions such as the formation of multiple lateral domains/grains in single layer AgSC15 during melting/quenching cycles can also partially explain the NanoDSC results in this study. Further experiments on more different species of AgSCn lamellae are necessary for a more complete understanding of the mechanism of layer evolution in layered systems upon fast heating/cooling cycles.

4. Conclusion

In summary, NanoDSC with fast heating (~50,000 K/s) and fast cooling (~10^4 K/s) rates is potentially useful in the *in situ* investigation of layer evolution of single layer AgSC15 *via* multiple melting/cooling cycles and electrical annealing, which is a potential alternative to furnace annealing in thin film growth.

The first NanoDSC pulse ($T_{max} > T_m$) shows the melting behavior of the as-synthesized lamella with well-defined crystallinity. The following quenching causes crystallinity loss, which results in a decrease of melting point, reduction of heat of fusion and broadening of melting peak FWHM. This effect persists in the subsequent melting/cooling cycles. Periodic electrical annealing to a temperature lower than the sample melting point ($T_{max} < T_m$) recovers the melting point of quenched samples to that of as-synthesized crystals. But the evolution of heat of fusion is irreversible after multiple melting/cooling cycles and never reaches that of the first pulse. Possible explanations involving chain-length-dependent melting as well as material desorption in single layer crystals are proposed.

As a comparison, conventional DSC with relatively low sensitivity can only be used to study bulk multilayer AgSC15 samples. No information on lamella structure evolution is obtained as the measurement is reversible due to slow scanning rate.

Acknowledgements

This work is supported by NSF-DMR-1006385, NSF-DMR-1409953 and University of Illinois Research Board (ID# 13187). The NanoDSC sensors are fabricated at the Cornell Nanoscale Science and Technology Facility (CNF), a member of the National Nanotechnology Infrastructure Network (NNIN). SEM measurement is carried out in the Frederick Seitz Materials Research Laboratory (MRL), University of Illinois. The authors thank Ms. N. Robards for the help with DSC measurements, which is conducted in the Ceramics Kiln House, University of Illinois.

References

[1] E.A. Olson, M.Y. Efremov, M. Zhang, Z.S. Zhang, L.H. Allen, The design and operation of a MEMS differential scanning nanocalorimeter for high-speed heat capacity measurements of ultrathin films, J. Microelectromech. Syst. 12 (2003) 355–364.
[2] M.Y. Efremov, E.A. Olson, M. Zhang, S. Lai, F. Schiettekatte, Z.S. Zhang, L.H. Allen, Thin-film MEMS differential scanning nanocalorimetry: heat capacity analysis, Thermochim. Acta 412 (2004) 13–23.
[3] M.Y. Efremov, E.A. Olson, M. Zhang, F. Schiettekatte, Z.S. Zhang, L.H. Allen, Ultrasensitive, fast, thin-film differential scanning calorimeter, Rev. Sci. Instrum. 75 (2004) 179.
[4] D.W. Denlinger, E.N. Abarra, K. Allen, P.W. Rooney, M.T. Messer, S.K. Watson, F. Hellman, Thin film microcalorimeter for heat capacity measurements from 1.5 to 800 K, Rev. Sci. Instrum. 65 (1994) 946–959.
[5] S.L. Lai, G. Ramanath, L.H. Allen, P. Infante, Z. Ma, High-speed (10^4(C/s) scanning microcalorimetry with monolayer sensitivity (J/m^2), Appl. Phys. Lett. 67 (1995) 1229–1231.
[6] F. Fominaya, T. Fournier, P. Gandit, J. Chaussy, Nanocalorimeter for high resolution measurements of low temperature heat capacities of thin films and single crystals, Rev. Sci. Instrum. 68 (1997) 4191–4195.
[7] R. Karmouch, Y. Anahory, J.-F. Mercure, D. Bouilly, M. Chicoine, G. Bentoumi, R. Leonelli, Y.Q. Wang, F. Schiettekatte, Damage evolution in low-energy ion implanted silicon, Phys. Rev. B 75 (2007) 075304.
[8] A.A. Minakov, C. Schick, Ultrafast thermal processing and nanocalorimetry at heating and cooling rates up to 1 MK/s, Rev. Sci. Instrum. 78 (2007) 073902.
[9] E. Zhuravlev, C. Schick, Fast scanning power compensated differential scanning nano-calorimeter: 1. The device, Thermochim. Acta 505 (2010) 1–13.
[10] E. Zhuravlev, C. Schick, Fast scanning power compensated differential scanning nano-calorimeter: 2. Heat capacity analysis, Thermochim. Acta 505 (2010) 14–21.
[11] M. Molina-Ruiz, A.F. Lopeandía, F. Pi, D. Givord, O. Bourgeois, J. Rodríguez-Viejo, Evidence of finite-size effect on the temperature in ultrathin layers of CoO nanograins, Phys. Rev. B 83 (2011) 140407.
[12] P. Swaminathan, D.A. LaVan, T.P. Weihs, Dynamics of solidification in Al thin films measured using a nanocalorimeter, J. Appl. Phys. 110 (2011) .
[13] M. Molina-Ruiz, A.F. Lopeandía, M. González-Silveira, Y. Anahory, M. Guihard, G. Garcia, M.T. Clavaguera-Mora, F. Schiettekatte, J. Rodríguez-Viejo, Formation of Pd_2Si on single-crystalline Si (1 0 0) at ultrafast heating rates: an in-situ analysis by nanocalorimetry, Appl. Phys. Lett. 102 (2013) 143111.
[14] F. Yi, D.A. LaVan, Electrospray-assisted nanocalorimetry measurements, Thermochim. Acta 569 (2013) 1–7.
[15] K. Xiao, J.M. Gregoire, P.J. McCluskey, J.J. Vlassak, A scanning AC calorimetry technique for the analysis of nano-scale quantities of materials, Rev. Sci. Instrum. 83 (2012) 114901.
[16] J.L. Garden, H. Guillou, A.F. Lopeandia, J. Richard, J.S. Heron, G.M. Souche, F.R. Ong, B. Vianay, O. Bourgeois, Thermodynamics of small systems by nanocalorimetry: from physical to biological nano-objects, Thermochim. Acta 492 (2009) 16–28.
[17] S.L. Lai, J.Y. Guo, V. Petrova, G. Ramanath, L.H. Allen, Size-dependent melting properties of small tin particles: nanocalorimetric measurements, Phys. Rev. Lett. 77 (1996) 99–102.
[18] S.L. Lai, J.R.A. Carlsson, L.H. Allen, Melting point depression of Al clusters generated during the early stages of film growth: nanocalorimetry measurements, Appl. Phys. Lett. 72 (1998) 1098–1100.
[19] M.Y. Efremov, F. Schiettekatte, M. Zhang, E.A. Olson, A.T. Kwan, R.S. Berry, L.H. Allen, Discrete periodic melting point observations for nanostructure ensembles, Phys. Rev. Lett. 85 (2000) 3560–3563.
[20] M. Zhang, M.Y. Efremov, F. Schiettekatte, E.A. Olson, A.T. Kwan, S.L. Lai, T. Wisleder, J.E. Greene, L.H. Allen, Size-dependent melting point depression of nanostructures: nanocalorimetric measurements, Phys. Rev. B 62 (2000) 10548–10557.
[21] E.A. Olson, M.Y. Efremov, M. Zhang, Z.S. Zhang, L.H. Allen, Size-dependent melting of Bi nanoparticles, J. Appl. Phys. 97 (2005) 34304.
[22] M.Y. Efremov, E.A. Olson, M. Zhang, Z. Zhang, L.H. Allen, Glass transition in ultrathin polymer films: calorimetric study, Phys. Rev. Lett. 91 (2003) 85703.
[23] Z.S. Zhang, O.M. Wilson, M.Y. Efremov, E.A. Olson, P.V. Braun, W. Senaratne, C.K. Ober, M. Zhang, L.H. Allen, Heat capacity measurements of two-dimensional self-assembled hexadecanethiol monolayers on polycrystalline gold, Appl. Phys. Lett. 84 (2004) 5198.
[24] R.K. Kummamuru, L. De La Rama, L. Hu, M.D. Vaudin, M.Y. Efremov, M.L. Green, D.A. LaVan, L.H. Allen, Measurement of heat capacity and enthalpy of formation of nickel silicide using nanocalorimetry, Appl. Phys. Lett. 95 (2009) 181911.
[25] M. Zhang, J. Wen, M.Y. Efremov, E.A. Olson, S. Zhang, L. Hu, L. De La Rama, R.K. Kummamuru, K.L. Kavanagh, Z. Ma, L.H. Allen, Metastable phase formation in the Au–Si system via ultrafast nanocalorimetry, J. Appl. Phys. 111 (2012) 93516.
[26] L.P. de la Rama, L. Hu, Z. Ye, M.Y. Efremov, L.H. Allen, Size effect and odd-even alternation in the melting of single and stacked AgSCn layers: synthesis and nanocalorimetry measurements, J. Am. Chem. Soc. 135 (2013) 14286–14298.
[27] K.S. Novoselov, A.K. Geim, S.V. Morozov, D. Jiang, Y. Zhang, S.V. Dubonos, I.V. Grigorieva, A.A. Firsov, Electric field effect in atomically thin carbon films, Science 306 (2004) 666–669.
[28] S.Z. Butler, S.M. Hollen, L. Cao, Y. Cui, J.A. Gupta, H.R. Gutiérrez, T.F. Heinz, S.S. Hong, J. Huang, A.F. Ismach, E. Johnston-Halperin, M. Kuno, V.V. Plashnitsa,

R.D. Robinson, R.S. Ruoff, S. Salahuddin, J. Shan, L. Shi, M.G. Spencer, M. Terrones, W. Windl, J.E. Goldberger, Progress, challenges, and opportunities in two-dimensional materials beyond graphene, ACS Nano 7 (2013) 2898–2926.
[29] B. Busupalli, S. Kummara, G. Kumaraswamy, B.L.V. Prasad, Ultrathin sheets of metal or metal sulfide from molecularly thin sheets of metal thiolates in solution, Chem. Mater. (2014) .
[30] J.J. Thomson, Application of Dynamics to Physics and Chemistry, McMillan, London, 1888.
[31] L. Hu, Z.S. Zhang, M. Zhang, M.Y. Efremov, E.A. Olson, L.P. de la Rama, R.K. Kummamuru, L.H. Allen, Self-assembly and ripening of polymeric silver-alkanethiolate crystals on inert surfaces, Langmuir 25 (2009) 9585–9595.
[32] L. Hu, L.P. de la Rama, M.Y. Efremov, Y. Anahory, F. Schiettekatte, L.H. Allen, Synthesis and characterization of single-layer silver decanethiolate lamellar crystals, J. Am. Chem. Soc. 133 (2011) 4367–4376.
[33] I.G. Dance, K.J. Fisher, R.M.H. Banda, M.L. Scudder, Layered structure of crystalline AgSR, Inorg. Chem. 30 (1991) 183–187.
[34] M.J. Baena, P. Espinet, M.C. Lequerica, A.M. Levelut, Mesogenic behavior of silver thiolates with layered structure in the solid-state – covalent soaps, J. Am. Chem. Soc. 114 (1992) 4182–4185.
[35] H.G. Fijolek, J.R. Grohal, J.L. Sample, M.J. Natan, A facile trans to gauche conversion in layered silver butanethiolate, Inorg. Chem. 36 (1997) 622–628.
[36] F. Bensebaa, T.H. Ellis, E. Kruus, R. Voicu, Y. Zhou, Characterization of self-assembled bilayers: silver-alkanethiolates, Langmuir 14 (1998) 6579–6587.
[37] R. Voicu, A. Badia, F. Morin, R.B. Lennox, T.H. Ellis, Structure and dynamics of selectively deuterated self-assembled silver n-octadecanethiolate layerered materials, Chem. Mater. 13 (2001) 2266–2271.
[38] R. Voicu, A. Badia, F. Morin, R.B. Lennox, T.H. Ellis, Thermal behavior of a self-assembled silver n-dodecanethiolate layered material monitored by DSC FTIR and ^{13}C NMR spectroscopy, Chem. Mater. 12 (2000) 2646–2652.
[39] A.A. Levchenko, C.K. Yee, A.N. Parikh, A. Navrotsky, Energetics of self-assembly and chain confinement in silver alkanethiolates: enthalpy–entropy interplay, Chem. Mater. 17 (2005) 5428–5438.
[40] R.T.W. Popoff, A.A. Zavareh, K.L. Kavanagh, H.-Z. Yu, Reduction of gold penetration through phenyl-terminated alkyl monolayers on silicon, J. Phys. Chem. C 116 (2012) 17040–17047.
[41] B. Radha, G. Liu, D.J. Eichelsdoerfer, G.U. Kulkarni, C.A. Mirkin, Layer-by-layer assembly of a metallomesogen by dip-pen nanolithography, ACS Nano 7 (2013) 2602–2609.
[42] L.P. de la Rama, L. Hu, M.Y. Efremov, E.A. Olson, P.F. Nealey, M.A. McLean, S.G. Sligar, L.H. Allen, Anomalous transitions of DODAB using fast scanning liquid calorimetry, Thermochim. Acta 522 (2011) 72–76.
[43] R.K. Kummamuru, L. Hu, L. Cook, M.Y. Efremov, E.A. Olson, L.H. Allen, A close proximity self-aligned shadow mask for sputter deposition onto a membrane or cavity, J. Micromech. Microeng. 18 (2008) 95027.
[44] S. van Herwaarden, E. Iervolino, F. van Herwaarden, T. Wijffels, A. Leenaers, V. Mathot, Design, performance and analysis of thermal lag of the UFS1 twin-calorimeter chip for fast scanning calorimetry using the Mettler-Toledo Flash DSC 1, Thermochim. Acta 522 (2011) 46–52.
[45] J. Elmer, E. Specht, Measurement of Sn and In solidification undercooling and lattice expansion using in situ X-ray diffraction, J. Electron. Mater. 40 (2011) 201–212 LA - English.
[46] A.T. Kwan, M. Efremov, E.A. Olson, F. Schiettekatte, M. Zhang, P.H. Geil, L.H. Allen, Nanoscale calorimetry of isolated polyethylene single crystals, J. Polym. Sci.: Part B: Polym. Phys. 39 (2001) 1237–1245.
[47] D.T. Grubb, J.J.H. Liu, M. Caffrey, D.H. Bilderback, Real time small-angle x-ray scattering during annealing of polymer single crystals, J. Polym. Sci.: Polym. Phys. Ed. 22 (1984) 367–378.
[48] L.C. Burmeister, Convective Heat Transfer, 2nd ed., Wiley-Interscience, 1993, pp. 107.